Article

Cell Reports

Macroautophagy Proteins Control MHC Class I Levels on Dendritic Cells and Shape Anti-viral CD8$^+$ T Cell Responses

Graphical Abstract

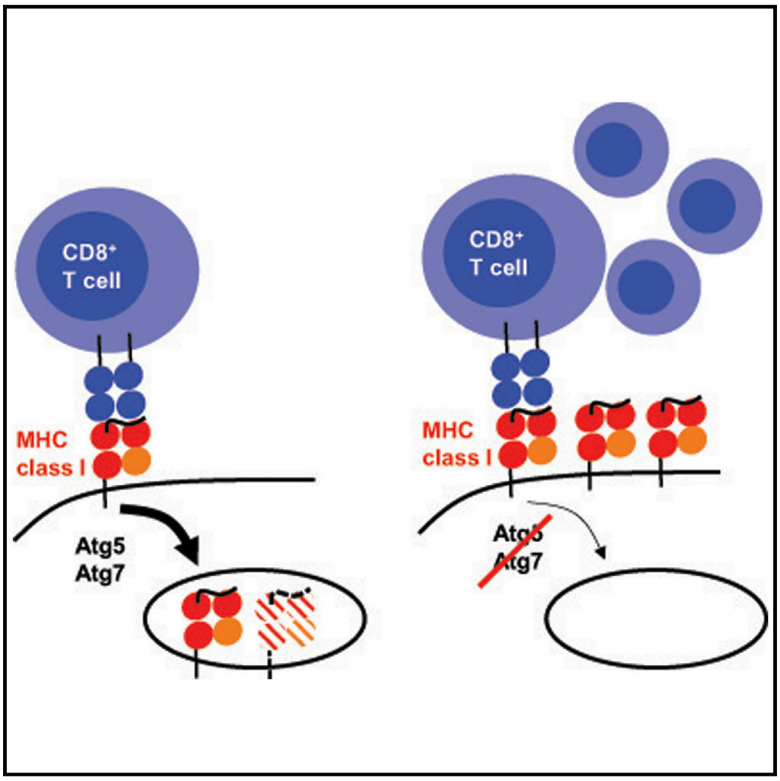

Authors

Monica Loi, Anne Müller, Karin Steinbach, ..., Doron Merkler, Christian Münz, Monique Gannagé

Correspondence

christian.muenz@uzh.ch (C.M.), monique.ghannage@unige.ch (M.G.)

In Brief

Macroautophagy assists in antigen processing for MHC class II presentation. In contrast to this supportive role for CD4$^+$ T cell stimulation, Loi et al. demonstrate that macroautophagy proteins diminish antigen presentation on MHC class I molecules during anti-viral CD8$^+$ T cell responses by supporting MHC class I internalization in dendritic cells.

Highlights

- Atg5- and 7-deficient dendritic cells (DCs) have increased surface MHC class I levels
- MHC class I internalization is compromised in the absence of Atg5
- In the absence of LC3 lipidation, AAK1 gets less efficiently recruited to MHC class I
- As a result, anti-viral CD8$^+$ T cell responses are more efficiently stimulated

Loi et al., 2016, Cell Reports *15*, 1076–1087
May 3, 2016
http://dx.doi.org/10.1016/j.celrep.2016.04.002

CellPress

OPEN ACCESS
CellPress

Cell Reports
Article

Macroautophagy Proteins Control MHC Class I Levels on Dendritic Cells and Shape Anti-viral CD8$^+$ T Cell Responses

Monica Loi,[1] Anne Müller,[1] Karin Steinbach,[2] Jennifer Niven,[2,3] Rosa Barreira da Silva,[1] Petra Paul,[1] Laure-Anne Ligeon,[1] Assunta Caruso,[2,3] Randy A. Albrecht,[4,6] Andrea C. Becker,[7] Nicolas Annaheim,[1] Heike Nowag,[1] Jörn Dengjel,[7] Adolfo García-Sastre,[4,5,6] Doron Merkler,[2,8] Christian Münz,[1,9,*] and Monique Gannagé[1,2,3,9,*]

[1]Viral Immunobiology, Institute of Experimental Immunology, University of Zürich, 8057 Zürich, Switzerland
[2]Department of Pathology and Immunology, School of Medicine, University of Geneva, 1211 Geneva, Switzerland
[3]Division of Rheumatology, Department of Internal Medicine, University Hospital, Geneva 1205, Switzerland
[4]Department of Microbiology, Icahn School of Medicine at Mount Sinai, New York, NY 10029, USA
[5]Department of Medicine, Division of Infectious Diseases, Icahn School of Medicine at Mount Sinai, New York, NY 10029, USA
[6]Global Health and Emerging Pathogens Institute, Icahn School of Medicine at Mount Sinai, New York, NY 10029, USA
[7]Department of Dermatology, Medical Center; ZBSA Center for Biological Systems Analysis; BIOSS Centre for Biological Signalling Studies; and FRIAS Freiburg Institute for Advanced Studies, University of Freiburg, 79104 Freiburg, Germany
[8]Department of Neuropathology, University Medical Center, 37099 Göttingen, Germany
[9]Co-senior author
*Correspondence: christian.muenz@uzh.ch (C.M.), monique.ghannage@unige.ch (M.G.)
http://dx.doi.org/10.1016/j.celrep.2016.04.002

SUMMARY

The macroautophagy machinery has been implicated in MHC class II restricted antigen presentation. Here, we report that this machinery assists in the internalization of MHC class I molecules. In the absence of the autophagy factors Atg5 and Atg7, MHC class I surface levels are elevated due to decreased endocytosis and degradation. Internalization of MHC class I molecules occurs less efficiently if AAK1 cannot be recruited via Atg8/LC3B. In the absence of Atg-dependent MHC class I internalization, dendritic cells stimulate CD8$^+$ T cell responses more efficiently in vitro and in vivo. During viral infections, lack of Atg5 results in enhanced influenza- and LCMV-specific CD8$^+$ T cell responses in vivo. Elevated influenza-specific CD8$^+$ T cell responses are associated with better immune control of this infection. Thus, the macroautophagy machinery orchestrates T cell immunity by supporting MHC class II but compromises MHC class I restricted antigen presentation.

INTRODUCTION

Macroautophagy is a major bulk degradative pathway in the cell, acting in parallel to the proteasome to degrade intracellular proteins and cell organelles (Mizushima et al., 2011). More than 30 autophagy related gene (*atg*) products form a double-membrane vesicle that engulfs cytoplasmic constituents bound to Atg8, an autophagy-related ubiquitin-like molecule that gets coupled to autophagosomal membranes. Yeast Atg8 has at least seven orthologs in higher eukaryotic cells, namely LC3A-C, GABARAP, and GABARAPL1-3. Initially thought to be a non-selective intracellular pathway of bulk degradation, there is now growing evidence that defines autophagy as a fine-tuned process with high cargo selectivity. Indeed, autophagy receptors, such as p62/sequestosome 1, optineurin, NBR-1, and NDP52, bind to substrates and recruit them to autophagosomal membranes, through binding of their LC3-interacting regions (LIRs) to Atg8 (Stolz et al., 2014). Autophagy substrates may comprise ubiquitinated proteins, N-terminally arginylated proteins, proteins with exposed glycosylation, and even organelles (Cha-Molstad et al., 2015; Randow and Münz, 2012). Macroautophagy is constitutively active in leukocytes and can mediate both adaptive and innate immune responses. During the innate immune response, various Toll- and NOD-like receptors (TLRs and NLRs) can enhance macroautophagy (Cooney et al., 2010; Delgado et al., 2009). The pathway also directly degrades intracellular pathogens, and some bacteria and viruses have evolved to develop strategies to escape autophagic degradation (Choi et al., 2013).

During the adaptive immune response, macroautophagy in antigen-presenting cells has been shown to directly control CD4$^+$ T cell responses, by regulating the delivery of both endogenous proteins and exogenous phagocytosed antigens to major histocompatibility complex (MHC) class II loading compartments (Lee et al., 2010; Schmid and Münz, 2007). Endogenous self-protein processing via macroautophagy contributes to both positive and negative CD4$^+$ T cell selection via presentation on MHC class II molecules in the thymus (Aichinger et al., 2013; Nedjic et al., 2008). This involves canonical macroautophagy and can be increased by selective targeting to autophagosomes via antigen fusion to LC3B. In contrast, exogenous antigen processing for MHC class II presentation seems to utilize the macroautophagy machinery via LC3-associated phagocytosis (LAP) (Ma et al., 2012; Romao et al., 2013). In this pathway, LC3B is coupled to

the cytosolic side of phagosomal membranes around cargo that has stimulated the recruitment of NADPH oxidase (NOX2) to the phagosomal membrane (Martinez et al., 2015; Romao et al., 2013). Reactive oxygen species production by NOX2 is required for LC3B recruitment to phagosomes, which, depending on the cell type, seems to accelerate or attenuate fusion with lysosomes. In the case of attenuation of lysosome fusion, MHC class II presentation of the endocytosed antigens seems to be prolonged (Romao et al., 2013).

Compared to antigen processing for MHC class II presentation, little is known about the mechanisms by which the macroautophagy machinery influences MHC class I restricted antigen presentation. Here, we report that antigen-presenting cells, like dendritic cells (DCs), which lack the core macroautophagy machinery that mediates Atg8 lipidation, have elevated surface MHC class I expression. This results from attenuated internalization and degradation of MHC class I molecules, and it involves the adaptor-associated kinase 1 (AAK1), which is recruited to MHC class I molecules via (presumably membrane-coupled) LC3B. MHC class I surface stabilization on DCs lacking Atg8 lipidation is associated with enhanced $CD8^+$ T cell responses during influenza A virus (IAV) and lymphocytic choriomeningitis virus (LCMV) infection, resulting in improved immune control of IAV. These findings establish a role for the macroautophagy machinery in controlling MHC class I expression and in shaping anti-viral $CD8^+$ T cell responses.

RESULTS

Increased MHC Class I Levels on Autophagy-Deficient *atg5*$^{-/-}$ or *atg7*$^{-/-}$ DCs and Macrophages In Vitro and In Vivo

In order to address whether MHC class I presentation could be affected by macroautophagy deficiency, we investigated mice in which *atg5* or *atg7* was conditionally deleted in DCs and CD11c-positive macrophages by crossing CD11c-cre mice with *atg5*- or *atg7*-floxed mice (*atg5*$^{-/-}$ or *atg7*$^{-/-}$ DC mice). Atg5 is a key component of the Atg8 E3-like ligase Atg5-Atg12-Atg16L1, required for autophagosome formation, and *atg7* encodes the E1-like enzyme for both Atg8 and Atg12 conjugation. We analyzed the surface levels of the MHC class I molecules H2-K^b and H2-D^b on *atg5*-deficient cells by flow cytometry. We found that *atg5*$^{-/-}$ DCs and alveolar macrophages displayed higher MHC class I cell surface expression at steady state than their *atg5*$^{fl/fl}$ littermates (Figures 1A and 1B), as well as compared to wild-type and CD11c-cre transgenic C57BL/6 mice (Figures S1B and S1C). Indeed, both H2-K^b and H2-D^b molecules of splenic $CD11c^+$ cells were expressed at significantly higher surface levels in *atg5*$^{-/-}$ DC mice (Figures 1A, 1B, and S1A). This elevated H2-K^b and H2-D^b expression was observed on both $CD11b^+$ and $CD8^+$ subsets of splenic DCs. In addition, MHC class I expression on tissue-resident $CD11c^+$ cells was also significantly higher in the absence of *atg5*. In the lungs, for example, H2-D^b expression on $CD11c^+$ alveolar macrophages and $CD11b^+$ and $CD103^+$ DCs was significantly higher on *atg5*$^{-/-}$ cells (Figures 1A and 1B). Moreover, *atg5*-deficient bone-marrow-derived DCs (BM-DCs) displayed higher MHC class I levels than their wild-type counterparts (Figure 1C). In contrast, MHC class I surface expression was unchanged on B and T cells (Figures 1D and S1D). These data were confirmed in *atg7*$^{-/-}$ DC mice. Although deletion efficiency seemed to be lower, resulting in residual LC3B lipidation in $CD11c^+$ cells of these mice (data not shown), MHC class I levels were elevated on Atg7-deficient macrophage and DC populations, but not B or T cells (Figures 1E, S1E, and S1F). These findings suggest that deficiency in the core machinery of macroautophagy, which is required for Atg8 lipidation, increases MHC class I levels on myeloid antigen-presenting cells.

In order to address the mechanisms that could lead to MHC class I upregulation in the absence of macroautophagy, we tested four hypotheses. First, we ruled out a difference in MHC class I gene expression, by quantifying MHC class I transcript levels in flow cytometrically sorted splenic *atg5*$^{+/+}$ and *atg5*$^{-/-}$ DCs (Figure 2A). No difference in MHC class I transcription was also confirmed in the investigated lung and splenic DC and macrophage subpopulations (Figure 2B). These data indicate that the increased MHC class I surface expression of macroautophagy-deficient DCs is not due to altered MHC class I gene transcription. We therefore addressed as the second hypothesis a difference in the availability of ubiquitinated substrates for proteasomal degradation and MHC class I loading. We could not detect any difference in the total amount of polyubiquitinated proteins in *atg5*$^{-/-}$ DCs compared to *atg5*$^{+/+}$ DCs by western blot quantification (data not shown). As the third hypothesis, a faster assembly or transport to the cell surface of new MHC class I-peptide complexes was assessed in *atg5*$^{-/-}$ DCs. This could result from different mechanisms, as follows: a compensatory proteasomal ligand generation, an increased proteasomal activity in the absence of autophagic degradation of this multi-catalytic protease, or an enhanced vesicular transport to the cell surface (Dengjel et al., 2012; Marshall et al., 2015). We did not see any difference in the rate of de novo expression of MHC class I molecules on the cell surface as assessed after acid stripping, which denatures surface MHC class I molecules, followed by measuring the kinetics of MHC class I recovery at the cell surface (Figures 2C and 2D). These results taken together suggest that the higher surface expression of MHC class I molecules on *atg5*$^{-/-}$ DCs is not related to enhanced gene transcription, increased availability of antigenic peptides, or elevated synthesis or trafficking of de novo formed MHC class I-peptide complexes.

Deficiency in the Macroautophagy Machinery Compromises MHC Class I Internalization by DCs

The fourth hypothesis explored a potentially attenuated internalization of MHC class I molecules in the absence of the macroautophagy core machinery. Indeed, we found that antibody-labeled MHC class I molecules were internalized at a slower rate in *atg5*$^{-/-}$ compared to *atg5*$^{+/+}$ DCs (Figures 3A and S1G), increasing the difference in surface-labeled H2-D^b and H2-K^b molecules between Atg-deficient and sufficient DCs over time (Figures 3B and S1H). Therefore, we concluded that a reduced internalization rate is responsible for higher surface expression of MHC class I molecules in *atg5*$^{-/-}$ DCs and increased stability of MHC class I complexes on the cell surface. In good agreement with these findings, the total amount of MHC

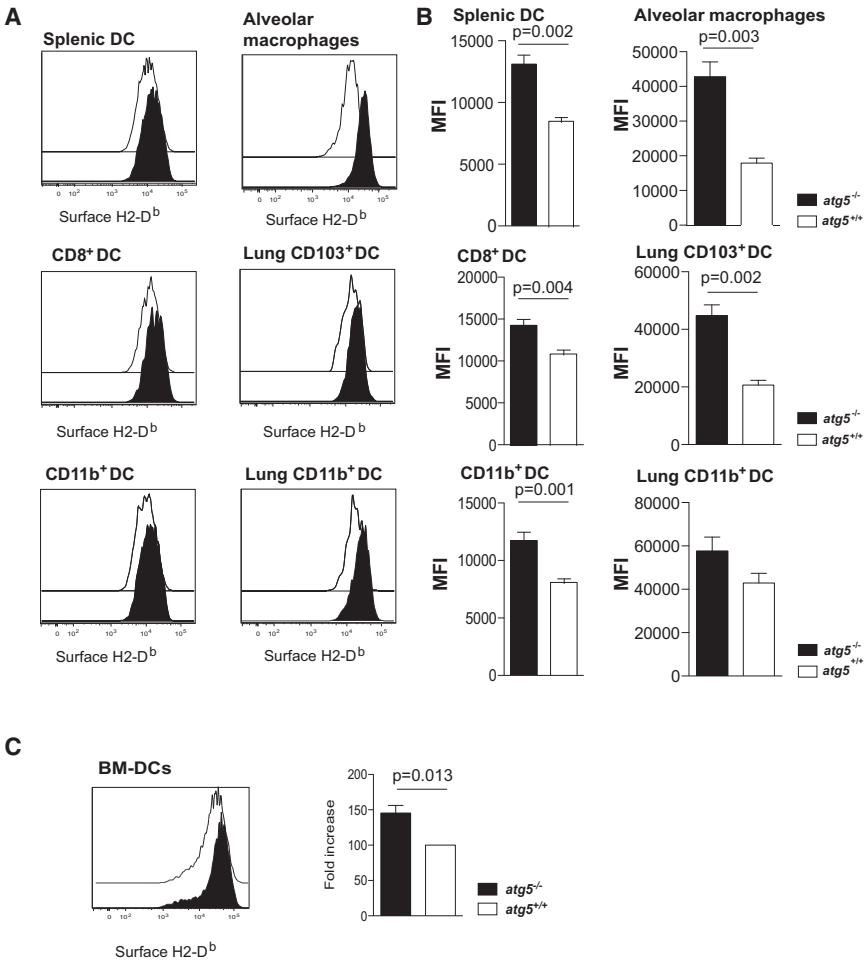

Figure 1. Elevated MHC Class I Expression on *atg5*- or *atg7*-Deficient DCs and Macrophages

(A) Expression of H2-D^b on *atg5*$^{+/+}$ and *atg5*$^{-/-}$ DCs and macrophages. Splenic DCs were gated as live CD11c$^+$ MHC class II^{high} cells, excluding inflammatory DCs and macrophages by using both Ly6C and F4/80 staining. Among these splenic DCs, H2-D^b expression on CD11b$^+$ and CD8$^+$ DCs was analyzed. Lung DCs were gated as live CD11c$^+$ MHC class II^{high} cells. DC subsets were further subdivided on the basis of CD11b and CD103 expression, and alveolar macrophages as double negative CD11b$^-$CD103$^-$ cells. Inflammatory DCs and monocytes were gated out using Ly6C staining. H2-D^b expression on alveolar macrophages, lung CD11b$^+$, and CD103$^+$ DCs was analyzed.

(B) Graphs summarize mean fluorescence intensity (MFI) values and SEM of H2-D^b from three independent experiments, each with three mice per group.

(C) Expression of H2-D^b on *atg5*$^{+/+}$ and *atg5*$^{-/-}$ BM-DCs. Representative flow cytometric staining (above) and all results (below) are from five independent experiments and are summarized as fold increase compared to *atg5*$^{+/+}$ DCs.

(D) MHC class I surface expression on B and T cells for the experiments of (A). Mean and SEM were plotted.

(E) Expression of MHC class I on *atg7*$^{+/+}$ and *atg7*$^{-/-}$ alveolar macrophages. Results are from six independent experiments and are summarized as fold increase compared to *atg7*$^{+/+}$ macrophages. Unpaired non-parametric two-tailed t tests were performed to obtain the indicated p values.

class I molecules was nearly 2-fold higher in extracts of *atg5*$^{-/-}$ splenic DCs than in the respective *atg5*$^{+/+}$ controls as determined by immunoblot quantification (Figures 3C and 3D), suggesting enhanced degradation of MHC class I molecules after internalization in the presence of the macroautophagy core machinery. In order to determine if this loss of internalization in the absence of Atg5 also affected other surface receptors, we tested the expression of CD29, CD44, transferrin receptor (TfR), the co-stimulatory molecules CD80 and CD86, and MHC class II. Only CD80 seemed to be regulated in a similar fashion as MHC class I, as it showed a tendency toward stabilization on the cell surface of some *atg5*$^{-/-}$ DC populations (mainly CD8$^+$ splenic DCs), while the surface expression of the other investigated receptors was unchanged during steady state as well as infection (Figures S2A–S2F). Furthermore, we also observed that vesicular MHC class I pools could not be formed in alveolar macrophages and DCs of *atg5*$^{-/-}$ and *atg7*$^{-/-}$ DC mice (Figures 3E, 3F, S2G, and S2H). Finally, lysosomal degradation of MHC class I was also attenuated in Atg5-deficient BM-DCs (Figures 3G and 3H). Treatment with the lysomotrophic agent chloroquine (CQ), elevating lysosomal pH and thereby inhibiting lysosomal hydrolases, accumulated MHC class I molecules in wild-type, but not in Atg5-deficient cells. In parallel LC3B-II also accumulated only in Atg5-positive DCs. Thus, the macroautophagy machinery assists in internalization and degradation of a subset of surface receptors, including MHC class I molecules, in DCs.

Atg Deficiency Compromises MHC Class I Association with AAK1, which Regulates MHC Class I Internalization

In order to analyze the molecular mechanism by which the macroautophagy machinery assists MHC I internalization and

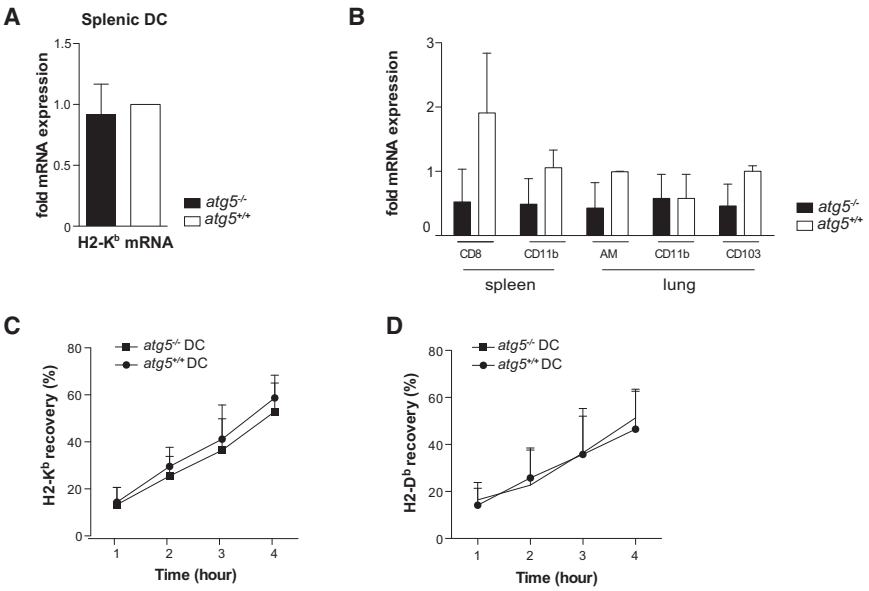

Figure 2. Similar MHC Class I Transcription and Transport to the Cell Surface in *atg5*$^{-/-}$-Deficient DCs

(A) Quantification of MHC class I transcript level in splenic *atg5*$^{+/+}$ and *atg5*$^{-/-}$ DCs. H2-K^b mRNA levels were determined by qRT-PCR in FACS sorted splenic DCs. Fold change in H2-K^b mRNA of *atg5*$^{-/-}$ cells compared to *atg5*$^{+/+}$ cells is represented (values are calculated using the 2exp-ΔΔct formula). Data combine three independent experiments.

(B) H2-K^b transcript levels in the indicated lung and splenic DC and macrophage (AM) populations. Data are from three mice per indicated experimental group.

(C and D) Restoration of H2-K^b (C) and H2-D^b (D) surface expression over time, in *atg5*$^{-/-}$ and *atg5*$^{+/+}$ DCs after acid stripping of surface molecules. Graphs represent the mean of three independent experiments.

degradation, we immunoprecipitated MHC class I molecules from *atg5*$^{+/+}$ murine embryonic fibroblasts (MEFs) and analyzed the results by mass spectrometry. We found the following two molecules that were previously reported to be involved in receptor-mediated endocytosis and degradation (data not shown): the AAK1 (Conner and Schmid, 2002) and the Ral A binding protein 1 (RALBP1) (Nakashima et al., 1999).

First, we confirmed the mass spectrometry results by immunoprecipitation and western blot analysis. We were able to identify both AAK1 and RALBP1 in MHC class I immune precipitates of both *atg5*$^{-/-}$ and *atg5*$^{+/+}$ BM-DCs (Figures 4A and S3A). However, only the association of AAK1 with MHC class I was significantly reduced in *atg5*$^{-/-}$ BM-DCs, compared to their wild-type counterparts (Figure 4A). In good agreement, AAK1 association with MHC class I molecules was also reduced in Atg7-deficient BM-DCs (Figure 4B). RNA silencing of AAK1 stabilized MHC class I levels on both MEFs and BM-DCs (Figures 4C, 4D, S3B, and S3C), confirming its previously published role during receptor internalization. Additionally, using the iLIR platform (Kalvari I et al., 2014; http://repeat.biol.ucy.ac.cy/iLIR/), we predicted two and one LIR motifs in the murine AAK1 and RALBP1 proteins, respectively (AAK1$_{118–123}$: DV**W**EV**L** [score 18], AAK1$_{914–919}$: DE**F**DP**I** [score 15], RALBP1$_{318–323}$: LS**W**LI**V** [score 16]). Interestingly, the LIR sequences are conserved in the human AAK1 protein, but not in human RALBP1. We validated the interactions of LC3 with AAK1 and RALBP1 by co-immunoprecipitations. Indeed, we found that both AAK1 (Figure 4E) and RALBP1 (Figure S3D) could be co-immunoprecipiated with LC3B, but this association did not seem to be influenced by the macroautophagy core machinery. These data suggest that LC3 lipidation via the macroautophagy core machinery is required to efficiently localize AAK1 to MHC class I molecules for optimal internalization and degradation.

Enhanced Antigen Presentation on Stabilized MHC Class I Molecules by Macroautophagy-Deficient DCs In Vitro

In order to correlate the enhanced MHC class I expression on *atg5*$^{-/-}$ DCs with better antigen presentation, we tested the ability of DCs deficient in the macroautophagy machinery to restimulate anti-viral CD8$^+$ T cell responses in vitro. We co-cultured IAV-infected *atg5*$^{+/+}$ or *atg5*$^{-/-}$ DCs with virus-specific polyclonal memory T cells isolated from IAV-infected wild-type animals. We found that infected *atg5*$^{-/-}$ DCs were able to expand IAV-specific memory CD8$^+$ T cells more efficiently than *atg5*$^{+/+}$ DCs (Figures 5A and 5B). This applied to both influenza nucleoprotein (NP)-specific and overall CD8$^+$ T cell populations. In contrast, IAV CD4$^+$ T cell expansion was not significantly different when stimulating with *atg5*$^{-/-}$ or *atg5*$^{+/+}$ influenza-infected DCs (Figure S4A). Moreover, NP1$_{366–374}$ peptide epitope pulsed *atg5*$^{-/-}$ DCs also expanded polyclonal IAV-specific memory T cells more efficiently than *atg5*$^{+/+}$ DCs (Figures 5C and 5D). Blocking CD80 during this in vitro restimulation did not significantly affect T cell proliferation. Therefore, we concluded that macroautophagy deficiency causes enhanced antigen presentation of MHC class I restricted IAV-derived epitopes by DCs.

Elevated CD8$^+$ T Cell Responses to Multiple IAV Antigens during Infection of Mice with DCs that Lack LC3 Lipidation

In order to validate our results in vivo, we infected *atg5*$^{-/-}$ DC mice and their wild-type littermates (*atg5*$^{+/+}$ DC mice) with a high dose (10 HAU) of IAV. The resulting CD8$^+$ T cell responses specific for influenza antigens (NP1, NP2, and hemagglutinin [HA]) were markedly enhanced in mice lacking the macroautophagy machinery in DCs. Indeed, the magnitude of the specific CD8$^+$ T cell response at day 11 post infection was two to four times greater in *atg5*$^{-/-}$ DC than in *atg5*$^{+/+}$

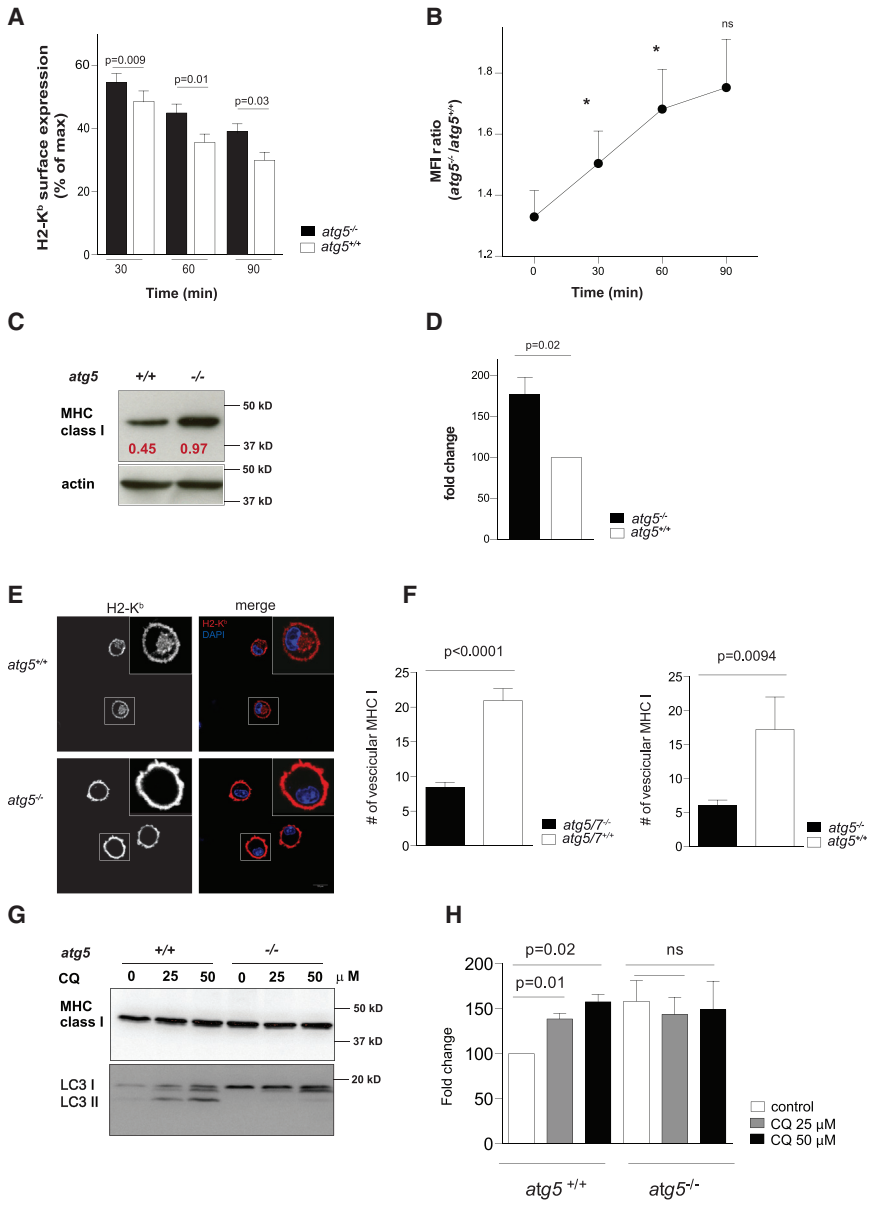

Figure 3. Atg Deficiency Compromises MHC Class I Internalization

(A) Internalization of MHC class I molecules over time in *atg5*$^{-/-}$ and *atg5*$^{+/+}$ DCs. Cells were labeled with anti-H2-K^b-specific antibodies and incubated at 37°C for the indicated times. The rate of internalization at 37°C of H2-K^b molecules was evaluated by the decrease of MFI intensity compared to the MFI of control DCs incubated at 4°C and set as a reference to 100%. p values are from paired non-parametric two-tailed t tests.

(B) The MFI ratio of H2-K^b surface staining on *atg5*$^{-/-}$ compared to *atg5*$^{+/+}$ DCs increases over time during incubation at 37°C. Statistics were performed using paired non-parametric two-tailed t tests to compare the MFI ratio (log values) of time 0 to 30 min ($p = 0.015$), to 60 min ($p = 0.01$), and to 90 min (ns, not significant). Graphs (A and B) are the summary of three independent experiments.

(C) Immunoblot analysis of MHC class I protein content in *atg5*$^{-/-}$ and *atg5*$^{+/+}$ splenic DCs. One representative immunoblot out of five is shown. Numbers below bands represent the ratio of normalized intensity of the MHC class I band compared to actin.

(D) Summary of the MHC class I quantification, normalized to actin, for all five immunoblots as described in (C).

(E) Immune fluorescence staining for H2-K^b on *atg5*$^{+/+}$ and *atg5*$^{-/-}$ lung CD11c$^+$ cells. Nuclear DNA was counterstained with DAPI. Scale bar indicates 10 μm.

(F) Quantification of vesicular (intracellular) MHC class I staining in lung CD11c$^+$ cells. Left: summary of *atg5*$^{+/+}$ and *atg5*$^{-/-}$ and *atg7*$^{+/+}$ and *atg7*$^{-/-}$ lung CD11c$^+$ cells. Right: quantification of *atg5*$^{+/+}$ and *atg5*$^{-/-}$ lung CD11c$^+$ cells. The presented data summarize three independent experiments.

(G) Immunoblot analysis of MHC class I protein content in *atg5*$^{-/-}$ and *atg5*$^{+/+}$ BM-DCs with and without chloroquine (CQ) treatment for 20 hr at concentrations of 25 and 50 μM. One representative immunoblot out of three is shown.

(H) Summary of the MHC class I quantification, normalized to actin, for all three immunoblots as described in (G). p values were determined by unpaired non-parametric two-tailed t tests.

DC mice (Figures 6A and 6B). In parallel, the specificity of the anti-viral CD8$^+$ T cell responses was broader in *atg5*$^{-/-}$ DC animals since at least two additional subdominant CD8$^+$ T cell epitopes ($HA_{211–225}$ and $NP2_{311–325}$) were recognized at frequencies reaching 10% of CD8$^+$ T cells apart from the dominant $NP1_{366–374}$ epitope in the C57BL/6 mouse background. Accordingly, recognition of subdominant IAV epitopes reached levels of wild-type dominant epitope recognition in *atg5*$^{-/-}$ DC mice.

Furthermore, we found that elevated CD8$^+$ T cell responses correlated with protection from IAV-induced disease. The infectious lung viral titers at day 8 were significantly reduced in *atg5*$^{-/-}$ DC mice (Figure 6C). Additionally, a significant correlation between the magnitude of the anti-viral CD8$^+$ T cell response and weight loss was observed (Figure 6D), indicating that the increased CD8$^+$ T cell responses in the absence of the macroautophagy core machinery protected from morbidity during IAV infection. The specific anti-viral CD4$^+$ T cell responses and the influenza-specific antibody titers were not significantly different in *atg5*$^{-/-}$ DC animals compared to their wild-type littermates (*atg5*$^{+/+}$ DC) (Figures S4B and S4C). In good agreement, MHC class I surface expression remained elevated on Atg 5-deficient DCs and macrophages during IAV infection (Figure S2E), while with the exception of CD80 co-stimulatory molecules were unchanged (Figure S2F). Thus, while the protective CD8$^+$ T cell response is selectively enhanced in infected mice with Atg5-deficient DCs, CD4$^+$ T cell and antibody responses are unaffected.

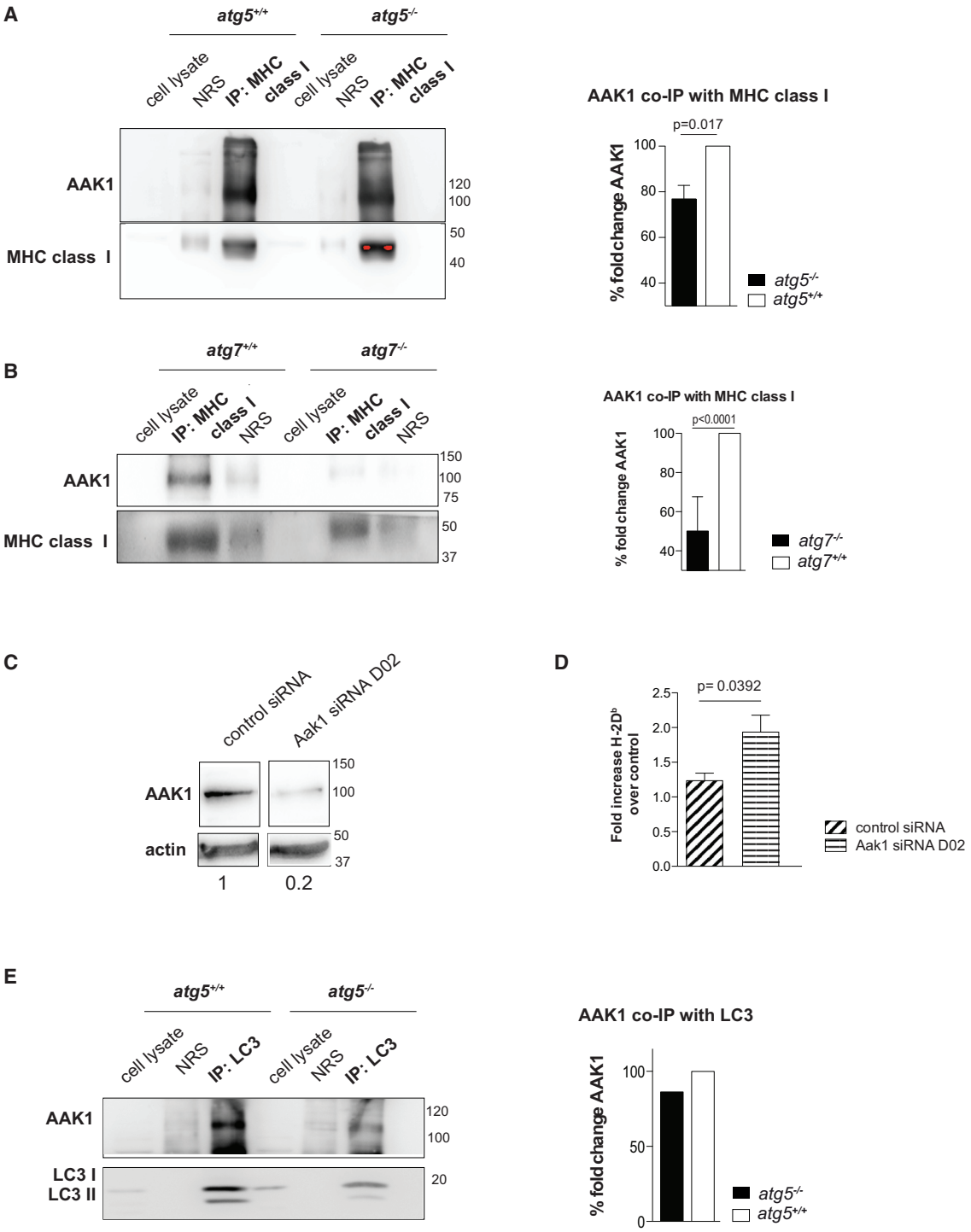

Figure 4. AAK1 Does Not Efficiently Associate with MHC Class I in the Absence of LC3B Lipidation

(A) AAK1 co-immunoprecipitation with MHC class I. Lysates of *atg5*$^{-/-}$ and *atg5*$^{+/+}$ BM-DCs were used to immunoprecipitate MHC class I. Left: representative western blot analysis showing the co-immunopreciptation of AAK1 with MHC class I. Right: quantification of five independent experiments. Co-immunoprecipitation intensity of AAK1 was normalized to MHC class I intensity. The AAK1 amount co-immunoprecipitated from the *atg5*$^{-/-}$ samples (n = 5, mean = 76.8%, SEM is 5.9) and the *atg5*$^{+/+}$ samples (set to 100% as a reference) were compared. p value shown is from an unpaired non-parametric two-tailed t test.

(B) Lysates of *atg7*$^{-/-}$ and *atg7*$^{+/+}$ BM-DCs were used to immunoprecipitate MHC class I. Left: representative western blot analysis showing the co-immunopreciptation of AAK1 with MHC class I. Right: quantification of three independent experiments. Co-immunoprecipitation intensity of AAK1 was normalized to MHC class I intensity. The AAK1 amount co-immunoprecipitated from the *atg7*$^{-/-}$ samples and the *atg7*$^{+/+}$ samples (set to 100% as a reference) were compared. p value shown is from an unpaired non-parametric two-tailed t test of the non-normalized values.

(legend continued on next page)

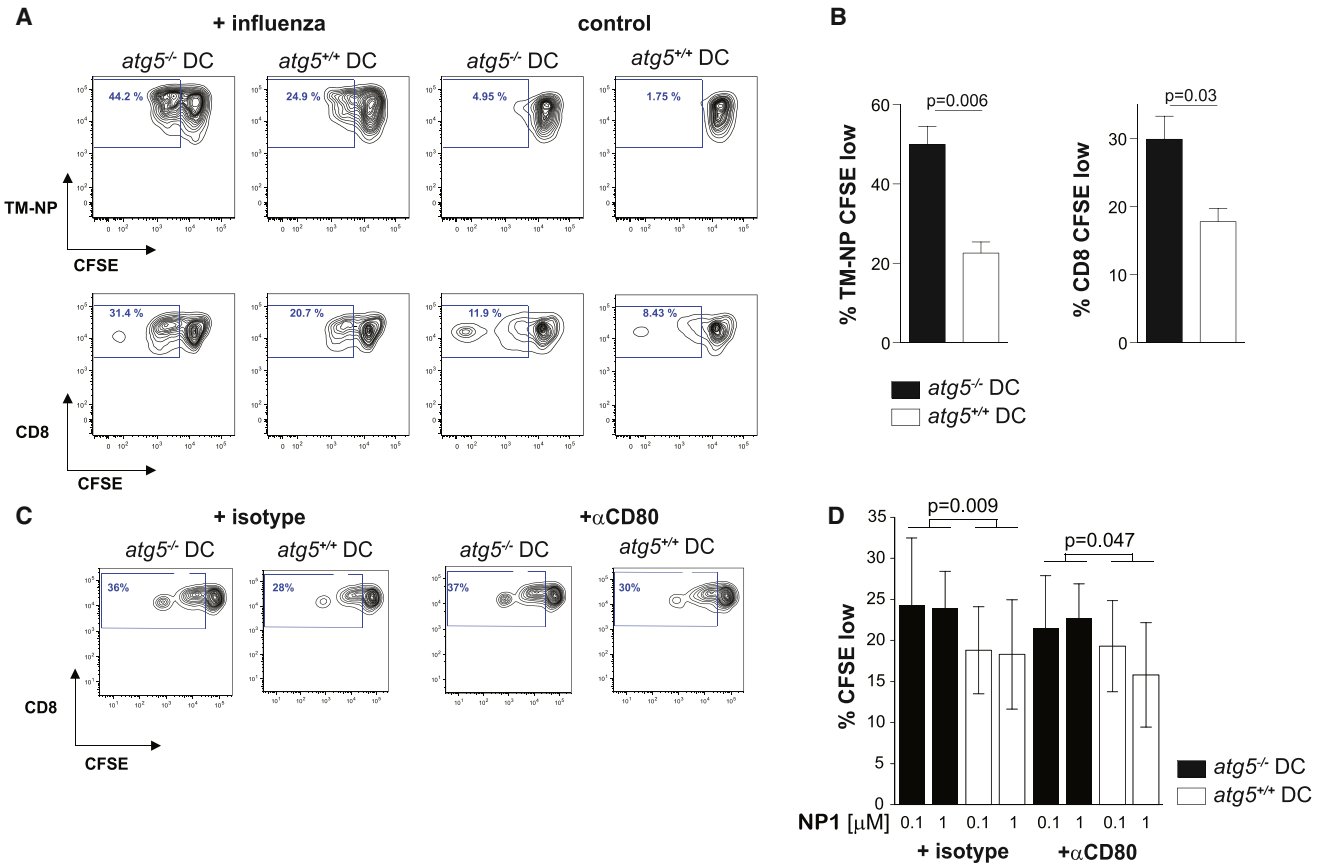

Figure 5. DCs Deficient in the Molecular Macroautophagy Machinery Have Greater Antigen Presentation Capacity to CD8$^+$ T Cells In Vitro

(A) IAV-infected or control *atg5*$^{-/-}$ and *atg5*$^{+/+}$ splenic DCs were co-cultured with CFSE-labeled influenza-virus-specific polyclonal memory T cells isolated from infected wild-type animals. T cell proliferation was determined after 3 days of co-culture by flow cytometry. Percent of CFSE low cells of influenza NP1$_{366–374}$/H2-D^b tetramer-positive (TM-NP, upper row) or total IAV-specific CD8$^+$ T cells (lower row) are indicated. One representative experiment out of three is shown.

(B) Graphical analysis of T cell proliferation from three independent experiments. p values were determined by unpaired non-parametric two-tailed t tests.

(C) NP1$_{366–374}$ *atg5*$^{-/-}$ or *atg5*$^{+/+}$ splenic DCs were co-cultured with CFSE-labeled influenza-virus-specific polyclonal memory T cells isolated from infected wild-type animals. T cell proliferation was determined after 3 days of co-culture with CD80 blocking antibody (+αCD80) or isotype control (+isotype) by flow cytometry. Percent of CFSE low cells of total CD8$^+$ T cells are indicated. One representative experiment out of three is shown.

(D) Summary of CD8$^+$ T cell proliferation assays with 0.1 and 1 μM NP1$_{366–374}$ peptide pulsed DCs as outlined in (C). p values were determined by paired two-tailed t tests.

Cytokine Production and Early Viral Titers in IAV-Infected Mice with DCs that Lack Components of the Macroautophagy Machinery

In order to exclude that changes in early innate immune control and cytokines would allow IAV to replicate to higher viral titers resulting in elevated IAV-specific CD8$^+$ T cell responses in *atg5*$^{-/-}$ DC mice, we analyzed cytokine production and IAV titers on day 3 after infection. Cytokine secretion in response to infection was similar for interleukin-6 (IL-6) and interferon-γ (IFN-γ) in *atg5*$^{-/-}$ DC mice (Figures S5A and S5B). IL-1β, however, was increased (Figure S5C), but these elevated IL-1β levels were not able to control IAV infection early on, as demonstrated by similar viral titers between wild-type and knockout mice on day 3 after infection (Figure S5D). Therefore, changes in innate immune control are unlikely to account for the elevated CD8$^+$ T cell responses and improved immune control in *atg5*$^{-/-}$ DC mice.

(C) Immunoblot for AAK1 on lysates from MEFs with (AAK1 small interfering RNA [siRNA] D02) and without (control siRNA) RNA silencing of AAK1. One representative of three experiments is shown.

(D) H2-D^b surface expression levels on MEFs after AAK1 silencing with AAK1-specific siRNA as well as control siRNA. Four experiments are summarized. p values were obtained from unpaired non-parametric two-tailed t tests.

(E) AAK1 co-immunoprecipitate with LC3. Lysates from *atg5*$^{-/-}$ and *atg5*$^{+/+}$ BM-DCs were used to immune precipitate LC3. Left: representative western blot analysis showing the co-immunoprecipitation of AAK1 with LC3. Right: quantification of three independent experiments. The co-immunoprecipitation intensity of AAK1 was normalized to the total LC3 (I and II). The amount of AAK1 co-immunoprecipitated from the *atg5*$^{-/-}$ samples (n = 3) and the *atg5*$^{+/+}$ samples (set to 100% as a reference) were compared. Statistical analysis was performed with an unpaired non-parametric two-tailed t test (ns, not significant).

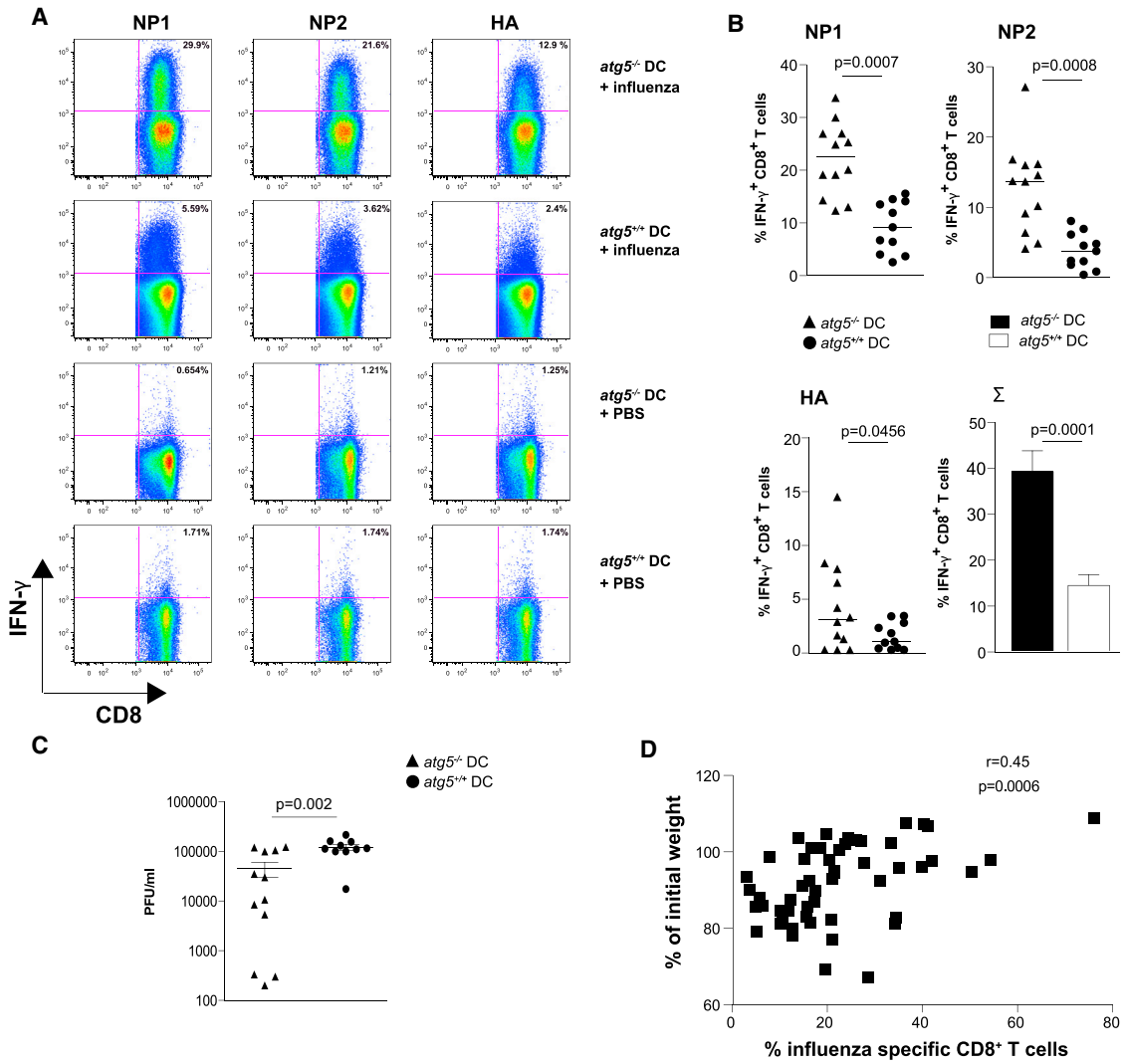

Figure 6. Broader Specificity and Enhanced Magnitude of Influenza-Specific CD8$^+$ T Cell Responses in Mice Lacking *atg5* in Their DCs

(A and B) Levels of influenza-virus-specific CD8$^+$ T cells in the lungs of wild-type mice (*atg5*$^{+/+}$ DC) and mice with *atg5*-deficient DCs (*atg5*$^{-/-}$ DC) were assessed 11 days after intranasal infection with 10 HA units of influenza virus strain A/PR8. Intracellular interferon-γ (IFN-γ) staining of CD8$^+$ T cells after in vitro peptide restimulation with three different viral epitopes (NP1$_{366–374}$, NP2$_{311–325}$, and HA$_{211–225}$) was determined by flow cytometry. Background secretion was subtracted for every peptide and was determined for every mouse by using an irrelevant peptide control (Ny-ESO-1$_{157–170}$). (A) Representative FACS plots of PBS mock-infected or influenza-infected mice. (B) Quantification of the specific anti-viral CD8$^+$ T cell responses to the three different viral epitopes (NP1, HA, and NP2) or their sum (Σ). Data are from three independent experiments, each with three to four mice per group. p values are from non-parametric unpaired two-tailed t tests.

(C) Influenza lung viral titers were determined at day 8 post influenza infection, from supernatants of total lung homogenates from *atg5*$^{-/-}$ or *atg5*$^{+/+}$ DC mice infected with 10 HAU of influenza A/PR8. Unpaired non-parametric two-tailed t tests were used to obtain the indicated p values.

(D) The magnitude of the anti-viral CD8$^+$ T cell response significantly inversely correlated with the weight loss at day 7 post influenza infection (p value is from Spearman non-parametric test). Data were obtained from six independent experiments: three with 10 HAU and three with 0.1, 0.5, or 1 HAU.

Elevated CD8$^+$ T Cell Responses to Two LCMV Epitopes during Infection of Mice with DCs Deficient in the Macroautophagy Machinery

In order to address the role of elevated MHC class I expression on *atg5*$^{-/-}$ DCs for better CD8$^+$ T cell priming in a different infectious model, we tested LCMV infection. *atg5*$^{-/-}$ DC animals and their wild-type littermates (*atg5*$^{+/+}$ DC) were infected intravenously (i.v.) with the wild-type LCMV Armstrong strain at a dose of 10^4 PFU. The specific CD8$^+$ T cell response to two viral epitopes was monitored at day 6 and day 11 post infection. We did not find a difference in the anti-viral CD8$^+$ T cell response at day 6 between the two groups (data not shown); however, at day 11, the anti-viral CD8$^+$ T cell response was significantly elevated in *atg5*$^{-/-}$ DC animals. The percentages of MHC class I tetramer-positive cells that are specific to two viral LCMV epitopes, the immunodominant H2-D^b-NP396 and the subdominant H2-K^b-GP34 epitope, were up to 2-fold higher in *atg5*$^{-/-}$ DC animals (Figures 7A and 7B). These data suggest

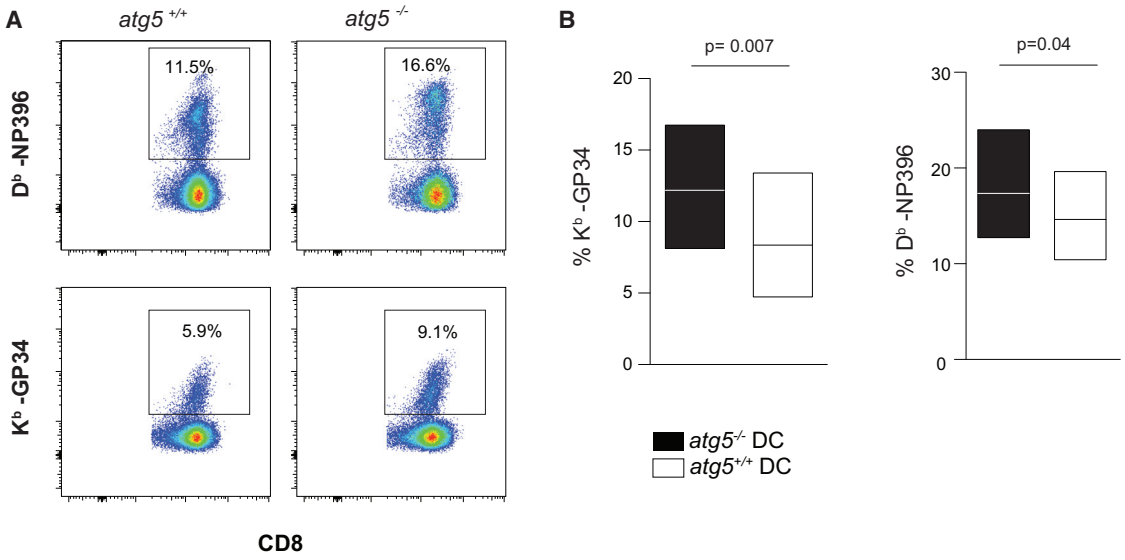

Figure 7. Enhanced LCMV-Specific CD8⁺ T Cell Responses in Mice Lacking the Macroautophagy Machinery in Their DCs

(A and B) *atg5*$^{-/-}$ DC animals and their wild-type littermates (*atg5*$^{+/+}$ DC) were infected intravenously (i.v.) with the wild-type LCMV Armstrong strain at a dose of 10^4 PFU. The specific CD8$^+$ T cell response to two viral epitopes was monitored in the blood, at day 11 post infection, using specific MHC class I tetramers. Data are from three independent experiments, each with three to four mice per group. (A) Percentage of MHC I tetramer-positive cells of CD8$^+$ T cells specific for the H2-D^b restricted $NP_{396–404}$ (D^b-NP396, upper row) or the H2-K^b restricted $GP_{34–43}$ (K^b-GP34, lower row) epitope in the blood of *atg5*$^{+/+}$ or *atg5*$^{-/-}$ DC mice. (B) Combined data as in (A) for all three experiments. Paired non-parametric two-tailed t tests were performed on the mean values from each experiment to obtain the indicated p values.

that stabilized MHC class I levels on macroautophagy-machinery-deficient DCs contribute to elevated priming of anti-viral CD8$^+$ T cell responses in vivo.

DISCUSSION

Our studies describe a role for lipidated LC3B in recruiting the internalization machinery to MHC class I molecules. In the absence of this recruitment, MHC class I gets stabilized on the surface of myeloid antigen-presenting cells. This results in elevated CD8$^+$ T cell responses during IAV and LCMV infections. Therefore, the macroautophagy machinery seems to attenuate MHC class I restricted antigen presentation, while it was previously shown to enhance MHC class II restricted antigen presentation.

MHC class I internalization seems to utilize at least two pathways. Recycling of MHC class I molecules has been shown to follow an ADP-ribosylation factor 6 (ARF6)-dependent endocytosis pathway (Naslavsky et al., 2004). This pathway is clathrin and dynamin independent. In contrast, AAK1, whose recruitment to MHC class I we found to be LC3B lipidation dependent, has been mainly implicated in clathrin- and dynamin-mediated endocytosis (Conner and Schmid, 2002; Henderson and Conner, 2007). The latter pathway seems to lead to lysosomal degradation of MHC class I and is also targeted by the K3 and K5 ubiquitin E3 ligases of the Kaposi sarcoma-associated herpesvirus (KSHV) (Coscoy et al., 2001; Hewitt et al., 2002). Interestingly, an ubiquitin mutant that affects this MHC class I internalization for degradation by K3 also affects MHC class I surface stability of cells that do not express these viral proteins (Duncan et al., 2010), suggesting that possibly membrane-associated RING-CH (MARCH) E3-ubiquitin ligases engage the same pathway. Indeed, MARCH4 and MARCH9 overexpression has been shown to stimulate MHC class I internalization for degradation (Nathan and Lehner, 2009). Thus, AAK1 recruitment via LC3B lipidation seems to assist MHC class I internalization for degradation, possibly enhancing an ubiquitin, clathrin- and dynamin-dependent internalization pathway. Compromising this internalization pathway seemed to also deplete the recently described vesicular MHC class I pools (Nair-Gupta et al., 2014), which were described to supply MHC class I molecules for cross-presentation of TLR engaging antigens. Interestingly, the macroautophagy machinery has been previously suggested to support clathrin-dependent endocytosis. Components of the AP2 complex, which is also directly phosphorylated by AAK1, have been found to interact with lipidated LC3B for Alzheimer precursor protein internalization and degradation (Tian et al., 2013). However, we did not find AP2 components significantly enriched in MHC class I immunoprecipitates (data not shown), and AAK1 can also support AP2-independent, but clathrin-dependent, endocytosis (Gupta-Rossi et al., 2011; Henderson and Conner, 2007). Thus, LC3B lipidation seems to affect different clathrin-dependent internalization and degradation steps of surface receptors, including MHC class I endocytosis.

We found that Atg-dependent MHC class I stabilization is associated with elevated CD8$^+$ T cell stimulation in vitro and in vivo. In addition, various contributions of the macroautophagy machinery to antigen processing for MHC class I presentation have been reported. While some studies found that Atg deficiency in antigen-presenting cells did not affect exogenous antigen cross-presentation to CD8$^+$ T cells (Lee et al., 2010), others

have shown that the macroautophagy machinery enhances (Fiegl et al., 2013; Mintern et al., 2015) or inhibits (Baghdadi et al., 2013; Hubbard-Lucey et al., 2014) cross-presentation. Moreover, it has been suggested that the macroautophagy machinery supports packaging of antigens in antigen donor cells for efficient cross-presentation (Li et al., 2008; Uhl et al., 2009). With respect to endogenous antigens, targeting of antigens to autophagosomes via fusion constructs with LC3B did not significantly enhance MHC class I presentation (Schmid et al., 2007), and macroautophagy seems to even restrict MHC class I antigen presentation of defective ribosomal products (Wenger et al., 2012). However, under conditions of inhibition of the classical MHC class I antigen processing pathway late in herpesvirus infections, it was reported that macroautophagy can deliver antigens for MHC class I presentation (English et al., 2009; Tey and Khanna, 2012). While most of these studies investigated the loss of components in the macroautophagy machinery in vitro, we and others have noted hyper-reactivity of $CD8^+$ T cell responses in the absence of Atgs in antigen-presenting cells (Hubbard-Lucey et al., 2014) and in colorectal tumor cells (Lévy et al., 2015), and we demonstrate in this study that MHC class I stabilization on DCs is associated with elevated anti-viral $CD8^+$ T cell responses in vivo. Nevertheless, we cannot exclude that in addition to MHC class I stabilization additional factors contribute to the increased $CD8^+$ T cell responses to viral infections in mice with Atg deficiency in DCs. Along these lines both the elevated CD80 surface expression on at least some subsets of DCs and the increased IL-1β production early during IAV infection could contribute.

Our study sheds light on the molecular mechanism of MHC class I internalization and degradation, involving recruitment of the internalization factor AAK1 via LC3B lipidation in this process. Thus, Atgs seem to balance MHC class I and II antigen presentation, being beneficial for $CD4^+$ T cell stimulation and restricting $CD8^+$ T cell responses at the same time. A comprehensive understanding of how the macroautophagy machinery interferes with MHC restricted antigen presentation seems required to predict the outcome of therapeutic interventions in this pathway to boost adaptive immunity.

EXPERIMENTAL PROCEDURES

Animals

8- to 12-week-old C57BL/6 (Janvier), *atg5*$^{flox/flox}$ (Hara et al., 2006), *atg7*$^{flox/flox}$ (Komatsu et al., 2005), and CD11c-Cre Tg (Jackson ImmunoResearch Laboratories) were bred in the UZH animal facility. All procedures used in the study complied with Swiss federal law for animal experimental procedures. All animal protocols were approved by the cantonal veterinary offices of the cantons of Zürich or of Geneva, Switzerland (protocol No. 117/2008, 134/2011, Medecine FRM 1005, and ZH210/2014).

Influenza Virus Infection In Vivo

Influenza A/PR8 virus (H1N1) virus was used for all experiments and purchased from Charles River. Mice were anesthetized and infected intra-nasally by the application of 25 μl of virus suspension (doses of virus were chosen between 0.1 and 10 HA units depending on the experiment).

Influenza Virus Infection In Vitro

$CD11c^+$ magnetic cell separation (MACS) sorted splenic DCs were infected at a MOI of 200 for 45 min in RPMI without serum.

LCMV Infection In Vivo

Animals were infected intravenously with the wild-type LCMV Armstrong strain at a dose of 10^4 PFU.

Mouse DCs

Splenic and lung $CD11c^+$ cells were isolated by positive magnetic cell separation (Miltenyi Biotec) and cultured in R10 (RPMI 1640 supplemented with 10% fetal calf serum [FCS]) and granulocyte-macrophage colony-stimulating factor (GM-CSF). Where indicated, $CD11c^+$ MHC class II^{high} cells were sorted on a FACS Aria Cell Sorter II (BD Biosciences).

BM-DCs were expanded using 20 ng/ml GM-CSF supplemented media and used at day 10. BM-DC purity was checked by FACS analysis, and if necessary (<80% $CD11c^+$ MHC class II^{high} cells), cells were enriched by positive CD11c selection.

Antibodies

Primary Antibodies for Flow Cytometry

The following mAbs were purchased from BD Biosciences or BioLegend (unless otherwise stated), as conjugated to phycoerythrin (PE), PE-Cy7, PerCP-Cy5.5, APC, APC-Cy7, Alexa Fluor 700, Pacific Blue, or biotin: anti-CD4(GK1.5), -CD8 (53-6.7), -CD11c (N418), -CD11b (M1/70), -F4/80 (BM8), -Ly6C (HK1.4), -CD103 (2E7), -CD80 (16-10A1), -CD86 (GL-1), -H2-K^b (AF6-88.5), -H2-D^b (KH95), -H2 class I (M1/42), -CD71 (RI7217) -CD80(16-10A1), -I-A/I-E (M5/114.15.2), and -IFN-γ (XMG1.2). For staining with biotinylated mAbs, samples were incubated with PE conjugated streptavidin. Anti-mouse CD16/32 for Fc receptor blocking was purchased from BD Biosciences. H2-D^b/ASNENMETM-PE tetramers were obtained from Immudex, and LCMV tetramers were purchased from TCmetrix. For detection of influenza infected cells, mouse monoclonal anti-influenza M2-E10 antibody was used (a gift from Dr. Tom Moran, New York, USA).

Primary Antibodies for Immunoblot Detection

The following primary antibodies were used: rabbit anti H2-K^b (Exon-8) (a gift from Dr. Jack Bennink, Bethesda, MD), anti-actin-HRP (Sigma-Aldrich), mouse anti-Atg5 (Nanotools), rabbit anti-LC3 (MBL International), mouse anti-LC3 (clone 5F10-Nanotools), rabbit anti-AAK1 (Abcam), and rabbit anti-RALBP1 (EMELCA).

Secondary Antibodies for Immunoblot Detection

The clean blot-HRP antibody (Life Technologies) and a goat-anti-mouse HRP (Bio-Rad) were used.

Peptides, Chemicals, and Inhibitors

Peptides were synthesized by GL Biochem at a purity > 90%. Carboxyfluorescein succinimidyl ester (CFSE) was used at 0.5 mM and was from Molecular Probes.

Flow Cytometry

Cells were acquired on a FACSFortessa flow cytometer using FACSDiva Version 6.1.3 software (BD Biosciences) or a FACSCanto II (BD Biosciences), and all flow cytometry analyses were performed with FlowJo Version 9.3.1 software (Treestar).

Influenza-Virus-Specific T Cell Proliferation

Influenza-specific polyclonal T cells were expanded from splenocytes of wild-type mice at day 12/14 post influenza infection, as previously described (Longhi et al., 2009), and cultured for 6/7 days in RPMI supplemented with 10% FCS and 40 units/ml of IL-2. For DC/T cell co-cultures, *atg5*$^{+/+}$ and *atg5*$^{-/-}$ splenic DC were influenza infected in vitro at a MOI of 200 and seeded overnight in R5 supplemented with GM-CSF or pulsed with 0.1 or 1 μM $NP1_{366–374}$ peptide for 1 hr. DCs were then co-cultured in 96 flat-bottom plates, at a 1/1 ratio with CFSE-labeled IAV-specific T cells (obtained from polyclonal T cell lines, or from lungs of wild-type infected animals). Co-culture with non-infected DCs was used as a control. Where indicated, CD80-specific blocking antibodies were added (10 μg/ml of clone 16-10A1) during the DC co-culture with T cells.

Intracellular IFN-γ Staining

Lung single-cell suspensions obtained after Percoll gradient centrifugation were incubated in R10 at 37°C for 5 hr in the presence of CD28- (2 μg/ml)

and influenza-specific peptides (10 μg/ml). Brefeldin A (10 μg/ml) was added after the first hour. Extracellular staining was performed (CD4, CD8, and live/dead Aqua). Then cells were fixed and permeabilized using a BD Cytofix Cytoperm Fixation/Permeabilization Kit and stained for IFN-γ.

ELISA Assay

For detection of cytokines in the lungs, lungs were weighted and resuspended in PBS (0.4 mg in 1.5 ml), then disrupted mechanically, using a Polytron. Homogenates were then centrifuged at 13,000 RPM for 30 min, and supernatants were tested for cytokine detection. Mouse Il-6 and IFN-γ ELISA kits were purchased from BioLegend. The mouse IL-1β ELISA kit was purchased from eBioscience or R&D.

MHC Class I Assays

Internalization assay was performed using anti-H2-D^b and anti-H2-K^b biotinylated antibodies. Briefly, CD11c MACS sorted DCs were stained in FACS buffer (PBS supplemented with 2% FCS and 0.01% Na azide) for 30 min at 4°C. Cells were washed two times in PBS, resuspended in R10, and kept at 4°C or incubated at 37°C for 30, 60, and 90 min. After the incubation time, cells were washed and surface staining was performed at 4°C with PE coupled streptavidin, anti-CD11c, anti-MHC class II, and Aqua.

Acid Stripping Assay

CD11c MACS sorted DCs were incubated for 2 min with ice-cold acid stripping buffer (131 mM sodium citrate, 66 mM sodium phosphate, and 1% BSA [pH 3]), then washed two times in R10 and kept at 4°C or incubated in R10 at 37°C for the indicated time points. After the incubation time, cells were washed and surface staining was performed at 4°C with anti-H2-D^b or anti-H2-K^b, anti-CD11c, anti-MHC II, and Aqua.

Immunoprecipitation

Lysates from BM-DCs were used at day 10 post differentiation. Cells were lysed in a 50 mM Tris-HCl [pH 7.5], 150 mM NaCl, 1% NP-40 buffer supplemented with protease inhibitors (Roche). Equal protein amounts from *atg5*$^{-/-}$ and *atg5*$^{+/+}$ lysates were used after bicinchoninic acid assay quantification. A minimum input of 1 mg was used per condition. Following a pre-clearing step of 1 hr, lysates were immunoprecipitated overnight at 4°C using either anti-MHC class I (exon8) or anti-LC3 (MBL International) antibodies. In parallel a rabbit control serum was used as a negative control. The next day cell lysates were further incubated with protein A beads (Pierce) for 2 hr. After five washes, beads were denaturated in SDS page loading buffer and co-immunoprecipitated proteins were analyzed by western blot. Immunoblot quantification was done using the Image J software.

Immune Fluorescence Microscopy

CD11c-positive cells were cultured overnight at 37°C in complete RPMI on coverslips. The next day, cells were washed in PBS three times and incubated with Fc blocker 2.4G2 Fcc III/II (BD Pharmingen) for 30 min at 4°C, followed by labeling for H2-K^b (antibody AF6-88.5) or H2 class I (antibody M1/42) for 30 min at 4°C. Next, they were incubated at 37°C for 1 hr, washed with PBS, and fixed in 4% paraformaldehyde 20 min at room temperature. Cells were washed with PBS, permeabilized with 0.1% Triton X-100, and saturated with 1% BSA for 1 hr. Binding of the primary antibody was detected with Alexa Fluor 555 goat anti-rat IgG H&L, and cell nuclei were stained with DAPI. Fluorescence was analyzed with a confocal laser scanning microscope.

Statistical Analysis

Statistical significance was tested by Student's t test with PRISM software (Version 5; GraphPad software). p values of less than 0.05 were considered statistically significant.

SUPPLEMENTAL INFORMATION

Supplemental Information includes Supplemental Experimental Procedures and five figures and can be found with this article online at http://dx.doi.org/10.1016/j.celrep.2016.04.002.

AUTHOR CONTRIBUTIONS

M.L., A.M., K.S., J.N., R.B.d.S., P.P., L.-A.L., A.C., A.C.B., N.A., and H.N. performed the experiments. R.A.A. and A.G.-S. provided crucial reagents. J.D., D.M., C.M., and M.G. planned and supervised the experiments. M.L., C.M., and M.G. wrote the manuscript.

ACKNOWLEDGMENTS

This work was supported by grants from Cancer Research Switzerland (KFS-3234-08-2013), Worldwide Cancer Research (14-1033), $KFSP^{MS}$ and $KFSP^{HHLD}$ of the University of Zurich, the Sobek Foundation, Fondation Acteria, the Swiss Vaccine Research Institute, and the Swiss National Science Foundation (310030_143979 and CRSII3_136241) to C.M. M.L. is funded by the Forschungskredit of the University of Zurich (K-41301-05-01). D. M. holds a stipendiary professorship of the Swiss National Science Foundation (No. PP00P3_152928). M.G. is supported by the Institute of Arthritis Research and the de Reuter foundation. R.A.A. and A.G.-S. are funded by the NIAID grant U19 AI117873, by CRIP (Center for the Research in Influenza Pathogenesis), and a NIAID-funded Center of Excellence in Influenza Research and Surveillance (CEIRS, contract no. HHSN272201400008C).

Received: September 28, 2015
Revised: January 10, 2016
Accepted: March 27, 2016
Published: April 21, 2016

REFERENCES

Aichinger, M., Wu, C., Nedjic, J., and Klein, L. (2013). Macroautophagy substrates are loaded onto MHC class II of medullary thymic epithelial cells for central tolerance. J. Exp. Med. *210*, 287–300.

Baghdadi, M., Yoneda, A., Yamashina, T., Nagao, H., Komohara, Y., Nagai, S., Akiba, H., Foretz, M., Yoshiyama, H., Kinoshita, I., et al. (2013). TIM-4 glycoprotein-mediated degradation of dying tumor cells by autophagy leads to reduced antigen presentation and increased immune tolerance. Immunity *39*, 1070–1081.

Cha-Molstad, H., Sung, K.S., Hwang, J., Kim, K.A., Yu, J.E., Yoo, Y.D., Jang, J.M., Han, D.H., Molstad, M., Kim, J.G., et al. (2015). Amino-terminal arginylation targets endoplasmic reticulum chaperone BiP for autophagy through p62 binding. Nat. Cell Biol. *17*, 917–929.

Choi, J.H., Cheong, T.C., Ha, N.Y., Ko, Y., Cho, C.H., Jeon, J.H., So, I., Kim, I.K., Choi, M.S., Kim, I.S., and Cho, N.H. (2013). Orientia tsutsugamushi subverts dendritic cell functions by escaping from autophagy and impairing their migration. PLoS Negl. Trop. Dis. *7*, e1981.

Conner, S.D., and Schmid, S.L. (2002). Identification of an adaptor-associated kinase, AAK1, as a regulator of clathrin-mediated endocytosis. J. Cell Biol. *156*, 921–929.

Cooney, R., Baker, J., Brain, O., Danis, B., Pichulik, T., Allan, P., Ferguson, D.J., Campbell, B.J., Jewell, D., and Simmons, A. (2010). NOD2 stimulation induces autophagy in dendritic cells influencing bacterial handling and antigen presentation. Nat. Med. *16*, 90–97.

Coscoy, L., Sanchez, D.J., and Ganem, D. (2001). A novel class of herpesvirus-encoded membrane-bound E3 ubiquitin ligases regulates endocytosis of proteins involved in immune recognition. J. Cell Biol. *155*, 1265–1273.

Delgado, M., Singh, S., De Haro, S., Master, S., Ponpuak, M., Dinkins, C., Ornatowski, W., Vergne, I., and Deretic, V. (2009). Autophagy and pattern recognition receptors in innate immunity. Immunol. Rev. *227*, 189–202.

Dengjel, J., Høyer-Hansen, M., Nielsen, M.O., Eisenberg, T., Harder, L.M., Schandorff, S., Farkas, T., Kirkegaard, T., Becker, A.C., Schroeder, S., et al. (2012). Identification of autophagosome-associated proteins and regulators by quantitative proteomic analysis and genetic screens. Mol. Cell. Proteomics *11*, 014035.

Duncan, L.M., Nathan, J.A., and Lehner, P.J. (2010). Stabilization of an E3 ligase-E2-ubiquitin complex increases cell surface MHC class I expression. J. Immunol. *184*, 6978–6985.

English, L., Chemali, M., Duron, J., Rondeau, C., Laplante, A., Gingras, D., Alexander, D., Leib, D., Norbury, C., Lippé, R., and Desjardins, M. (2009). Autophagy enhances the presentation of endogenous viral antigens on MHC class I molecules during HSV-1 infection. Nat. Immunol. *10*, 480–487.

Fiegl, D., Kägebein, D., Liebler-Tenorio, E.M., Weisser, T., Sens, M., Gutjahr, M., and Knittler, M.R. (2013). Amphisomal route of MHC class I cross-presentation in bacteria-infected dendritic cells. J. Immunol. *190*, 2791–2806.

Gupta-Rossi, N., Ortica, S., Meas-Yedid, V., Heuss, S., Moretti, J., Olivo-Marin, J.C., and Israël, A. (2011). The adaptor-associated kinase 1, AAK1, is a positive regulator of the Notch pathway. J. Biol. Chem. *286*, 18720–18730.

Hara, T., Nakamura, K., Matsui, M., Yamamoto, A., Nakahara, Y., Suzuki-Migishima, R., Yokoyama, M., Mishima, K., Saito, I., Okano, H., and Mizushima, N. (2006). Suppression of basal autophagy in neural cells causes neurodegenerative disease in mice. Nature *441*, 885–889.

Henderson, D.M., and Conner, S.D. (2007). A novel AAK1 splice variant functions at multiple steps of the endocytic pathway. Mol. Biol. Cell *18*, 2698–2706.

Hewitt, E.W., Duncan, L., Mufti, D., Baker, J., Stevenson, P.G., and Lehner, P.J. (2002). Ubiquitylation of MHC class I by the K3 viral protein signals internalization and TSG101-dependent degradation. EMBO J. *21*, 2418–2429.

Hubbard-Lucey, V.M., Shono, Y., Maurer, K., West, M.L., Singer, N.V., Ziegler, C.G.K., Lezcano, C., Motta, A.C.F., Schmid, K., Levi, S.M., et al. (2014). Autophagy gene Atg16L1 prevents lethal T cell alloreactivity mediated by dendritic cells. Immunity *41*, 579–591.

Komatsu, M., Waguri, S., Ueno, T., Iwata, J., Murata, S., Tanida, I., Ezaki, J., Mizushima, N., Ohsumi, Y., Uchiyama, Y., et al. (2005). Impairment of starvation-induced and constitutive autophagy in Atg7-deficient mice. J. Cell Biol. *169*, 425–434.

Lee, H.K., Mattei, L.M., Steinberg, B.E., Alberts, P., Lee, Y.H., Chervonsky, A., Mizushima, N., Grinstein, S., and Iwasaki, A. (2010). In vivo requirement for Atg5 in antigen presentation by dendritic cells. Immunity *32*, 227–239.

Lévy, J., Cacheux, W., Bara, M.A., L'Hermitte, A., Lepage, P., Fraudeau, M., Trentesaux, C., Lemarchand, J., Durand, A., Crain, A.M., et al. (2015). Intestinal inhibition of Atg7 prevents tumour initiation through a microbiome-influenced immune response and suppresses tumour growth. Nat. Cell Biol. *17*, 1062–1073.

Li, Y., Wang, L.X., Yang, G., Hao, F., Urba, W.J., and Hu, H.M. (2008). Efficient cross-presentation depends on autophagy in tumor cells. Cancer Res. *68*, 6889–6895.

Longhi, M.P., Trumpfheller, C., Idoyaga, J., Caskey, M., Matos, I., Kluger, C., Salazar, A.M., Colonna, M., and Steinman, R.M. (2009). Dendritic cells require a systemic type I interferon response to mature and induce $CD4^+$ Th1 immunity with poly IC as adjuvant. J. Exp. Med. *206*, 1589–1602.

Ma, J., Becker, C., Lowell, C.A., and Underhill, D.M. (2012). Dectin-1-triggered recruitment of light chain 3 protein to phagosomes facilitates major histocompatibility complex class II presentation of fungal-derived antigens. J. Biol. Chem. *287*, 34149–34156.

Marshall, R.S., Li, F., Gemperline, D.C., Book, A.J., and Vierstra, R.D. (2015). Autophagic Degradation of the 26S Proteasome Is Mediated by the Dual ATG8/Ubiquitin Receptor RPN10 in Arabidopsis. Mol. Cell *58*, 1053–1066.

Martinez, J., Malireddi, R.K., Lu, Q., Cunha, L.D., Pelletier, S., Gingras, S., Orchard, R., Guan, J.L., Tan, H., Peng, J., et al. (2015). Molecular characterization of LC3-associated phagocytosis reveals distinct roles for Rubicon, NOX2 and autophagy proteins. Nat. Cell Biol. *17*, 893–906.

Mintern, J.D., Macri, C., Chin, W.J., Panozza, S.E., Segura, E., Patterson, N.L., Zeller, P., Bourges, D., Bedoui, S., McMillan, P.J., et al. (2015). Differential use of autophagy by primary dendritic cells specialized in cross-presentation. Autophagy *11*, 906–917.

Mizushima, N., Yoshimori, T., and Ohsumi, Y. (2011). The role of Atg proteins in autophagosome formation. Annu. Rev. Cell Dev. Biol. *27*, 107–132.

Nair-Gupta, P., Baccarini, A., Tung, N., Seyffer, F., Florey, O., Huang, Y., Banerjee, M., Overholtzer, M., Roche, P.A., Tampé, R., et al. (2014). TLR signals induce phagosomal MHC-I delivery from the endosomal recycling compartment to allow cross-presentation. Cell *158*, 506–521.

Nakashima, S., Morinaka, K., Koyama, S., Ikeda, M., Kishida, M., Okawa, K., Iwamatsu, A., Kishida, S., and Kikuchi, A. (1999). Small G protein Ral and its downstream molecules regulate endocytosis of EGF and insulin receptors. EMBO J. *18*, 3629–3642.

Naslavsky, N., Weigert, R., and Donaldson, J.G. (2004). Characterization of a nonclathrin endocytic pathway: membrane cargo and lipid requirements. Mol. Biol. Cell *15*, 3542–3552.

Nathan, J.A., and Lehner, P.J. (2009). The trafficking and regulation of membrane receptors by the RING-CH ubiquitin E3 ligases. Exp. Cell Res. *315*, 1593–1600.

Nedjic, J., Aichinger, M., Emmerich, J., Mizushima, N., and Klein, L. (2008). Autophagy in thymic epithelium shapes the T-cell repertoire and is essential for tolerance. Nature *455*, 396–400.

Randow, F., and Münz, C. (2012). Autophagy in the regulation of pathogen replication and adaptive immunity. Trends Immunol. *33*, 475–487.

Romao, S., Gasser, N., Becker, A.C., Guhl, B., Bajagic, M., Vanoaica, D., Ziegler, U., Roesler, J., Dengjel, J., Reichenbach, J., and Münz, C. (2013). Autophagy proteins stabilize pathogen-containing phagosomes for prolonged MHC II antigen processing. J. Cell Biol. *203*, 757–766.

Schmid, D., and Münz, C. (2007). Innate and adaptive immunity through autophagy. Immunity *27*, 11–21.

Schmid, D., Pypaert, M., and Münz, C. (2007). Antigen-loading compartments for major histocompatibility complex class II molecules continuously receive input from autophagosomes. Immunity *26*, 79–92.

Stolz, A., Ernst, A., and Dikic, I. (2014). Cargo recognition and trafficking in selective autophagy. Nat. Cell Biol. *16*, 495–501.

Tey, S.K., and Khanna, R. (2012). Autophagy mediates transporter associated with antigen processing-independent presentation of viral epitopes through MHC class I pathway. Blood *120*, 994–1004.

Tian, Y., Chang, J.C., Fan, E.Y., Flajolet, M., and Greengard, P. (2013). Adaptor complex AP2/PICALM, through interaction with LC3, targets Alzheimer's APP-CTF for terminal degradation via autophagy. Proc. Natl. Acad. Sci. USA *110*, 17071–17076.

Uhl, M., Kepp, O., Jusforgues-Saklani, H., Vicencio, J.M., Kroemer, G., and Albert, M.L. (2009). Autophagy within the antigen donor cell facilitates efficient antigen cross-priming of virus-specific $CD8^+$ T cells. Cell Death Differ. *16*, 991–1005.

Wenger, T., Terawaki, S., Camosseto, V., Abdelrassoul, R., Mies, A., Catalan, N., Claudio, N., Clavarino, G., de Gassart, A., Rigotti, Fde.A., et al. (2012). Autophagy inhibition promotes defective neosynthesized proteins storage in ALIS, and induces redirection toward proteasome processing and MHCI-restricted presentation. Autophagy *8*, 350–363.